Quang-Van Doan[1,2], Fei Chen[2], Hiroyuki Kusaka[1], Anurag Dipankar[3], Ansar Khan[4], Rafiq Hamdi[5], Matthias Roth[6], Dev Niyogi[7]

[1] Center for Computational Sciences, University of Tsukuba, Japan

[2] Research Application Laboratory, National Center for Atmospheric Research, scientific visitor, USA

[3] Institute for Atmospheric and Climate Science, ETH Zurich, Switzerland

[4] Department of Geography, Lalbaba College, University of Calcutta, India

[5] Royal Meteorological Institute of Belgium, Belgium

[6] Department of Geography, National University Singapore, Singapore

[7] Jackson School of Geosciences, and Cockrell School of Engineering, University of Texas at Austin, USA

Corresponding author: Quang-Van Doan (doan.van.gb@u.tsukuba.ac.jp)

Key Points:

- New normal of "wet gets wetter and dry remains dry" in future city-scale precipitation is revealed.
- The intensification of extreme precipitation can reach the maximum at the "super" Clausius-Clapeyron ($\geq +7\%$ per K warming) rate.
- Extreme precipitation enhancement is attributed to the increased atmospheric moisture and, importantly, the enhanced lifting force.

Abstract

Understanding the response of extreme precipitation (EP) at a city scale to global warming is critical to protect a city from the risks of urban flooding under climate change. Yet, current knowledge on this issue is limited. Here, focusing on an urban agglomeration in the tropics, Singapore, we reveal that future global warming enhances both frequency and intensity of EP, based on simulations with a state-of-the-art convection-permitting regional climate model. EP intensification can reach maximum "super" Clausius-Clapeyron ($\geq +7\%$ per K warming) rate, consistently for both Representative Concentration Pathways (RCPs) 8.5 and 4.5. The intensification is lower for moderate and light precipitation, implying a situation of "wet gets wetter and dry remains dry". EP enhancement is attributed to the increased atmospheric moisture and, more importantly, the enhanced lifting force, which directly strengthens the precipitation-making processes.

Plain Language Summary

Understanding the response of extreme precipitation (EP) at a city scale to global warming is critical to protect a city from the risks of urban flooding under climate change. Here we show that future global warming will enhance both frequency and intensity of EP, based on simulations with a state-of-the-art

convection-permitting regional climate model for an urban agglomeration in the tropics, Singapore. EP intensification can reach maximum "super" Clausius-Clapeyron ($\geq$ +7% per K warming) rate, but lower for moderate and light precipitation, implying a "new normal" of "wet gets wetter and dry remains dry". EP enhancement is attributed to the increased atmospheric moisture and, more importantly, the enhanced lifting force, which directly strengthens the precipitation-making processes.

1 Introduction

Recent decades have witnessed an increased occurrence of natural disasters, including floods associated with extreme precipitation (EP) in cities("AR5 Climate Change 2014," n.d.). Making cities safe, resilient, and sustainable is one of United Nations Sustainable Development Goals 2030 (SDG2030, especially Goal 11)(United Nations, 2015). Achieving this goal is a challenge because cities are exposed to changing large-scale climatic feedbacks, and cities themselves are creating their microclimate. Such multiscale climatic forcing is causing non-stationarity in the climate system, which results in an increasing trend of unprecedented extreme weather and climate events that might occur in the future (Diffenbaugh et al., 2017; Fischer et al., 2021). As a result, urban areas that are designed based on historical hydroclimate conditions continue to be exposed to higher risk due to climate impacts, especially urban floods. Indeed, it is recognized that for some regions, precipitation extremes will become more frequent, more widespread, and/or more intense during the 21st century, and cities will be disproportionately at higher risk (Meyer et al., 2020).

A basis of framing the precipitation change due to climate warming is through the classical Clausius-Clapeyron (CC) relation (Fowler et al., 2021; Lenderink & van Meijgaard, 2009). The CC equation defines the saturation specific humidity of the atmosphere as a function of temperature. Hence, specific humidity near the Earth's surface is anticipated to rise at a rate of approximately 7% per degree warming (K^{-1}). Several past studies have shown that both short- ($<$ 1 day) and long-duration ($>$1 day) precipitation extremes intensify at a rate consistent with the increase in atmospheric moisture (~7% K^{-1})(Allan & Soden, 2008). In some regions, however, the increase in short-duration extreme rainfall intensity does not follow the expected CC relation (Fischer & Knutti, 2016; Guerreiro et al., 2018; Rajczak & Schär, 2017; Scherrer et al., 2016; Westra et al., 2014), there remains uncertainty regarding the response of short-duration precipitation extremes to global warming (Berg et al., 2013; Deser et al., 2012; Lenderink & Meijgaard, 2010; Lenderink & van Meijgaard, 2009; Panthou et al., 2014; Park & Min, 2017; Shepherd, 2014).

Several past studies have pointed out the impact of global warming on heavy precipitation. However, studies exploring the future changes in EP at small spatiotemporal scales, especially over cities are limited, due to limited data and computational resources required for conducting city-scale relevant meteorological simulations. Another reason relates to the large uncertainties involved in our understanding of processes at the city scale, which can influence short-term

precipitation. Such uncertainties include socio-economic forecasts, greenhouse emission scenarios, global climate models (GCMs) errors, and lack of physical parameterization schemes representing complex urban thermodynamics processes. At the city scale, the challenges are further compounded as the coarse resolution of current GCMs makes it impossible to explicitly represent convection processes and the interaction of mesoscale regimes, which are known to affect rainfall processes(Prein et al., 2017). Thus, dynamical downscaling methods are widely applied to partially overcome the scale issue by using kilometer-scale climate models to capture the local effects but retain the atmospheric forcing generated by GCMs. With this approach, mesoscale effects originating from urban-rural heterogeneities, cities, land/sea boundaries, or topography are better represented in the model. Nevertheless, uncertainties still exist and sometimes might be amplified, particularly in the precipitation process, which is very nonlinear and sensitive to multiple, multiscale forcings (Kusaka et al., 2016).

The present study focuses on tropical cities which are particularly vulnerable. They are home to 39 % of total urban dwellers globally (United Nations, 2018), usually located in fast-growing economies. Characterized by rapid urbanization and industrialization, they are likely more vulnerable to climate changes than their counterparts in higher-latitude areas (World Bank, 2010). Impacts of heavy rain and urban floods on socioeconomic well-being are particularly noteworthy due to the propensity for tropical warm-rain processes including from monsoons. As a result, there is a pressing need to understand better how EP changes with climate change and anthropogenic global warming in tropical cities to design for climate resilience properly.

Here, we assess the climatic response of EP at a city scale to global warming using Singapore as an example. The primary question of interest is: how will EP change in the future? More specifically, we address two research questions regarding city-scale EP change: (i) does the local EP show a significant global warming signal, and (ii) what atmospheric processes are responsible for eventual EP changes? We employ a state-of-the-art convection-permitting regional climate model based on the Weather Research Forecasting (WRF) modeling system, whose performance to simulate EP is verified against in-situ observed and satellite-derived rainfall products. Using dynamical downscaling, future EP climates until 2100 are simulated using Representative Concentration Pathways (RCPs) 8.5 and 4.5, respectively.

2 Materials and Methods

2.1 Model configuration

A convection-permitting regional climate model, named Weather Research and Forecast (W. C. Skamarock et al., 2008) (WRF), is used to simulate current-time and future precipitation climates over the Singapore region. The model is designed to have three nested domains with horizontal resolutions of 30 x 30, 6 x 6, and 2 x 2 km for gradually inheriting the large-scale atmospheric forcing while resolving the localized convective processes. The

innermost domain, having the size of 154 x 154 grid cells, covers the Singapore metropolitan area, the Southern Malaysia peninsula, and a part of the Indonesian islands (Fig. S1). The physical schemes of WRF (shown in Table 1) are selected for their being widely used in regional climate simulations (https://www2.mmm.ucar.edu/wrf/users/physics/phys_references.html). Note that the cumulus parameterization scheme is applied for the outermost domain only because fine resolutions of the inner domains allow them to resolve the convection processes explicitly. For modeling the urban effect, the single-layer urban canopy model (Kusaka et al., 2001; Kusaka & Kimura, 2004) is activated within the Noah land surface modeling (Chen et al., 2011) framework. To better representing the urban area, up-to-date urban land cover information (Demuzere et al., 2021) is used and overlaid over the default USGS land use database provided by WRF (Fig. S2). Urban parameters used in the simulations are kept as default as provided by WRF.

2.2 Experimental design

We conducted three separate simulations using different climate scenarios while keeping the same surface conditions (Table 2). The first simulation, i.e., the baseline climate (BC), reproduces the current climate. Two sensitive simulations, i.e., the future climate (FC), are aimed to dynamically downscale future climate assumed global warming up the end of the 21st century following two Representative Concentration Pathways (RCP) 8.5 and 4.5 (van Vuuren et al., 2011). In detail, simulation BC is forced by ERA-Interim reanalysis data (Dee et al., 2011) as initial and boundary conditions (IBCs) and run for November 2005 – 2014. November is selected because it falls into the inter-monsoon period (between the Southwest and Northeast monsoon seasons) when the prevailing wind is relatively weak, and the wet atmosphere is dominantly characterized by localized thunderstorms, at times severe (Doan et al., 2021; Fong & Ng, 2012; Simón-Moral et al., n.d.). Such atmospheric conditions are believed the most suitable for this study.

On the other hand, the FC simulations are forced by IBCs created using the pseudo-global warming (PGW) approach. PGW is a widely used dynamical downscaling method for investigating the response of localized weather to the global warming effect (Doan & Kusaka, 2018; Gutmann et al., 2018; Hibino et al., 2018; Lauer et al., 2013; Pall et al., 2017; Rasmussen et al., 2011; Sato et al., 2007; Schär et al., 1996). In PGW, RCMs are forced by "pseudo" future atmospheric conditions, defined as present-time reanalysis data added by so-called global warming increments (GWIs)(Doan & Kusaka, 2018). First, we calculate GWIs as anomalies between the future and current climate (in terms of monthly mean), provided by a GCM or ensemble of GCMs, for primary atmospheric variables, i.e., surface and air temperature, geopotential, wind (two components). GWIs are then re-gridded and added onto the reanalysis data of interest to be handled by RCMs. Details of the technical procedure of PGW as well as its advantages and disadvantages are well documented in previous literatures (Doan & Kusaka, 2018; Rasmussen et al., 2011; Sato et al., 2007).

A reason for selecting the PGW dynamical downscaling is because the method can isolate the primary signal of the global warming effect. PGW literately ignores the potential change in inter-annual and daily variabilities of the future climate system [31](Lauer et al., 2013; Sato et al., 2007). This characteristic allows us to focus exclusively on how warming background climate modifies extreme precipitation. The secondary impacts of global warming, such as the impacts of potential changes in weather variabilities, are intentionally not included in this study.

In terms of technical details, GWIs in this study are calculated as anomalies between the future and the reference climate data provided by CMIP5 GCMs (Meehl et al., 2009; Taylor et al., 2012). The future climate is defined as November mean for 20 years 2080 – 2099; meanwhile, the reference climate is 2000 – 2019. Three atmospheric variables, i.e., air temperature, geopotential height, and wind (two components) and one surface variable, i.e., surface temperature, are used. Two emission scenarios, that is, RCP4.5 and RCP8.5, are selected for the sake of covering inter-scenario uncertainty. To reduce the GCM-related bias, the ensemble mean of multiple GCMs are used instead of a single GCM. In detail, 36 GCMs for RCP8.5 and 30 GCMs for RCP4.5 are used for calculating the mean. GWIs values are then re-gridded and added over 6-hourly ERA-Interim reanalysis data to generate IBCs for WRF.

2.3 Rainfall data

In-situ measurement rainfall data used to evaluate the model's performance are from five manned weather stations, named Changi, Paya Lebar, Seletar, Sembawang and Tengah (S-24, S-06, S-25, S-80, and S-23). These stations are managed by the Meteorological Service Singapore (MSS). Rainfall values are hourly totals (e.g., 01:00 LT rainfall is that backward accumulated between 00:01 and 01:00 LT). A quality check is conducted by comparing against both tipping buckets and radar images (http://www.weather.gov.sg/learn_observations/).

Satellite precipitation product - CMORPH (CPC MORPHing technique) (NCEP, 2021) is used to compare with the WRF-driven precipitation data. CMORPH is useful because of its spatial coverage and can be used as complementary to in-situ measurement to verify the WRF results. CMORPH is global precipitation analysis at very high spatial and temporal resolution. This technique uses precipitation estimates derived from low orbiter satellite microwave observations exclusively and whose features are transported via spatial propagation information obtained entirely from geostationary satellite IR data. CMORPH has been bias corrected and reprocessed using the Climate Prediction Center (CPC) Morphing Technique (MORPH) to form a global, high resolution precipitation analysis. Data is reprocessed on a global grid with 8 x 8 km spatial resolution with temporal resolution is 30 minutes from January 1998–present.

3 Results

The performance of WRF on regional precipitation and its extremes is evaluated

against both in-situ measurements and satellite-derived precipitation products (CMORPH). The model agrees well with observations regarding the probability distribution of hourly precipitation across almost all precipitation intensities (Fig. 1a). The quantile-quantile (Q-Q) comparison provides a more specific comparison between the observed and modeled rainfall (Fig. 1b). Overall, the model slightly underestimates measured precipitation, especially at very high quantiles. NOAA's satellite-derived NOAA CPC Morphing Technique (CMORPH) data (Joyce et al., 2004) is used to expand 'observed' rainfall coverage. For direct comparison, the WRF output is upscaled to the resolution of the satellite product (to 8 x 8 km). The agreement between the model and CMORPH is relatively less, with the model overestimating high precipitation quantiles (up to 80%) and underestimating low quantiles (Fig. 1c, d). However, the overestimation of high precipitation quantiles is expected because of the relatively coarse resolution of the CMORPH product, which tends to smooth out fine-scale extreme precipitation (NCEP, 2021). Considering this known absolute bias, the agreement in the diurnal cycle and spatial variation of rainfall between WRF and CMORPH is reasonable (Fig. S3). Precipitation occurs at night and early morning over the Malacca Strait's open water and develops late afternoon and evening over the inland area.

"Rich get richer, and poor remains poor."

The question related to the future change is investigated by examining the difference between simulations for baseline climate (BC) and future climate (FC) (read Method for more details about simulation setting). Several interesting features stand out. First, the comparison shows a notable increase in the simulated EP in the future, namely an increase in event frequency and enhanced precipitation intensity (Fig. 2). Second, the characteristics of the changes are different with different precipitation types, revealing a more significant increase for heavy precipitation compared to lighter precipitation. For example, the occurrence probability of precipitation under 10 mm hr-1 is projected to increase by 10% (under scenario RCP8.5). In contrast, for precipitation greater than 30 mm hr-1, the increase can reach 50% or greater (Fig. 2a lower panel). The increasing trend is consistently seen for two RCP scenarios. However, the extent of the change is different between RCPs, with lesser with RCP4.5 and higher with RCP8.5. Interestingly, there is almost no inter-scenario difference for light precipitation, which becomes more pronounced for heavier precipitation.

In addition to the frequency, the changes in intensity are essential because of their urban flood implications. An interesting trend is seen as the more substantial intensification is likely to happen at upper-quantile precipitations. For example, with RCP8.5, precipitation of quantiles 0.95 and 0.99 are anticipated to increase by 3.3 and 5.8 mm/hr from 18.9 and 33.4 mm/hr in the present climate, corresponding to the increasing rates of 17.4 and 17.6%, respectively, for the land area. Also, the intensity change shows is RCP scenario dependent (Fig. 2a, d). The absolute increase of quantile 0.95 and 0.99 for RCP8.5 is roughly double that for RCP4.5. Further, while it varies among land, sea, and city, the

variation is relatively small compared to inter-scenario differences. Nevertheless, precipitation intensification is highest over water, followed by land area and most minor changes over the city (Fig. 2d).

Assessing the precipitation changes taking the C-C and rainfall change relation (~ 7% for 1K warming) as a reference can help provide insightful understanding about the climatic response (Fowler et al., 2021). It is interesting to note that despite variations in absolute values (Fig. 2d left panel), changes in rainfall intensities are likely to converge regardless of the RCP scenario. The asymmetric trend is seen among different quantiles (Fig. 2d right panel). The upper quantiles show more remarkable changes in terms of the CC rate. Over the sea, the change rate even reaches above 1.0, i.e., the "super" CC rate. Together with the changes in precipitation frequency, a consistent finding emerges: the heavier the current precipitation is, the more intense and frequent it will be in the future. For less heavy rainfall, the changes are expected to be minor and insignificant. This phenomenon is similar to resource redistribution of wealth in the social stratification theory (Angle, 1986), i.e., with more "wealth" (moisture supply), "the rich will get richer, and the poor remain poor".

The increase in future precipitation generally and especially in extremes is attributed to two possible factors if excluding the impacts of aerosol. The first is an increase in atmospheric moisture (the "fuel" for convective potential). The second is an enhanced vertical motion that lifts low-level moisture upward and favors more vigorous convection and more precipitation. The change in the atmospheric moisture is analyzed by examining the differences in total precipitable water between FC and BC (PW, Fig. 3). For example, FC RCP8.5 exhibits a 14 mm, or approximately 24%, increase compared to BC. A weaker increase is noted under FC RCP4.5 as well. This trend is inline across sea, land, city, and precipitation types, i.e., moderate and heavy.

On the other hand, the changes in convective available potential energy (CAPE) and convective inhibition (CIN) vary among precipitation types and land covers. CAPE indicates atmospheric instability and a necessary condition for generating convections. In contrast, CIN indicates suppression of convection development, which inhibits air parcels from rising from the surface to the level of free convection. Not surprisingly, results revealed a noticeable increase in CAPE in the future (up to 30 - 40 % with RCP8.5), indicating that a warmer atmosphere will provide a more favorable environment for convection (CAPE, Fig. 3). However, CIN also shows a positive trend, meaning that the "negative" force to suppress convection development is also enhanced (CIN, Fig. 3). But the absolute value of CIN is small to suppress convection. Instead, it helps to make convection vigorous by delaying it until lifting force overcomes CIN (Emanuel, 1994; Stull, 2016). One interesting fact worthy to note is that higher CAPE and lower CIN trends are seen for light precipitation (lower than quantile 0.5) compared to extreme precipitation (higher than quantile 0.9, 0.99). This result is somewhat counter-intuitive as if we expect that the atmosphere instability is a driven force of precipitation over the region of interest. Results for lifting force, in terms of

maximum vertical wind speed (W_max), provide a different insight. Overall, W_max with light precipitation is very small compared to extreme precipitation (W_max, Fig. 3). On the other hand, W_max during heavy and extreme precipitation is very high (~ 3 m /s), and further increases in the future. This result implies that the change in lifting force, but not CAPE, might play a more critical role in the story of extreme precipitation. Indeed, the diurnal cycle of rainfall for different thresholds (Fig. S4) shows a decrease in the frequency of extreme precipitation over the land area, particularly in the afternoon despite CAPE being highest.

4 Discussions and conclusions

This study presents the first results of future changes in extreme precipitation in a coastal, tropical urban agglomeration, Singapore, up to 2100, based on simulation results with the convection-permitting WRF model. It is clear that future global warming substantially enhances the frequency and intensity of extreme hourly precipitation at a city scale, primarily because the warmer atmosphere holds more moisture, the "fuel" of precipitation. More interestingly, the enhancement is not uniform among precipitation at different intensities, given the same increasing rate of atmospheric water vapor. The more extreme precipitation is intensified further in the future warming environment. Notably, intensified rate of very extreme one (greater than quantile 0.99) can reach "supper" Clausius-Clapeyron rate (greater than +7% per K). In contrast, the intensification of moderate and light precipitation (lower than quantile 0.5) is lower and close to zero Clausius-Clapeyron rate. This situation, metaphorically, can be expressed as "rich becomes richer and poor remains poor", given the same "wealth" (i.e., the same increased amount of atmospheric moisture). The result is significant for urban planners. The asymmetric nature of the future enhancement of precipitation has to be considered in mitigating more severe urban flash flooding caused by increased. This is especially important for coastal cities over the low-latitude tropical area, where sea-level rise, another impact of global warming, is known to be more serious (Spada et al., 2013).

Several uncertainties remain in this study. First, as we isolate the primary thermodynamic signal of global warming by employing the PGW approach for dynamical downscaling, it means that we ignore secondary signals such as potential changes in inter-annual variabilities or changes in large-scale weather patterns which could influence the extreme precipitation climate. However, comprehensively including global warming impacts in the sense of direct dynamical downscaling could blur the first signal of global warming on localized precipitation, making it difficult to derive a clear conclusion. We also do not discuss the model's physical-scheme-related uncertainty and those related to future changes in urban surface conditions or the impact of aerosols. Several sensitivity experiments with a different physical scheme and urban settings show that the discrepancy existing among these model settings does not affect this study's main conclusions. In this sense, though in this study we found that the signal from the city is likely different from those from the land and sea, this finding

fell into some uncertainty. Thus, how the urban effect on localized precipitation will change (increase/decrease) as the atmosphere becomes warmer, still open, and worthy to be answered in a future comprehensive assessment.

Acknowledgments

This research is funded by JSPS KAKENHI Grant Number 20K13258; JSPS KAKENHI Grant Number 19H01155; Multidisciplinary Cooperative Research Program in Center for Computational Sciences, University of Tsukuba; NASA IDS Grant # 80NSSC20K1262; USDA NIFA Grants 2015-67003-23460.

Open Research

The source code of WRF model Version 3.5.1 used in this paper can be downloaded from https://www2.mmm.ucar.edu/wrf/users/downloads.html. Codes used to set up model simulations, analyze data, and create figures can be provided upon request from the corresponding author.

References

Allan, R. P., & Soden, B. J. (2008). Atmospheric Warming and the Amplification of Precipitation Extremes. *Science*, *321*(5895), 1481–1484. https://doi.org/10.1126/science.1160787AR5 Climate Change 2014: Impacts, Adaptation, and Vulnerability — IPCC. (n.d.). Retrieved August 23, 2021, from https://www.ipcc.ch/report/ar5/wg2/Berg, P., Moseley, C., & Haerter, J. O. (2013). Strong increase in convective precipitation in response to higher temperatures. *Nature Geoscience*, *6*(3), 181–185. https://doi.org/10.1038/ngeo1731Dee, D. P., Uppala, S. M., Simmons, A. J., Berrisford, P., Poli, P., Kobayashi, S., et al. (2011). The ERA-Interim reanalysis: configuration and performance of the data assimilation system. *Quarterly Journal of the Royal Meteorological Society*, *137*(656), 553–597. https://doi.org/10.1002/qj.828Deser, C., Phillips, A., Bourdette, V., & Teng, H. (2012). Uncertainty in climate change projections: the role of internal variability. *Climate Dynamics*, *38*(3), 527–546. https://doi.org/10.1007/s00382-010-0977-xDiffenbaugh, N. S., Singh, D., Mankin, J. S., Horton, D. E., Swain, D. L., Touma, D., et al. (2017). Quantifying the influence of global warming on unprecedented extreme climate events. *Proceedings of the National Academy of Sciences*, *114*(19), 4881–4886.Doan, Q.-V., & Kusaka, H. (2018). Projections of urban climate in the 2050s in a fast-growing city in Southeast Asia: The greater Ho Chi Minh City metropolitan area, Vietnam. *International Journal of Climatology*, *38*(11), 4155–4171. https://doi.org/10.1002/joc.5559Doan, Q.-V., Dipankar, A., Simón-Moral, A., Sanchez, C., Prasanna, V., Roth, M., & Huang, X.-Y. (2021). Urban-induced modifications to the diurnal cycle of rainfall over a tropical city. *Quarterly Journal of the Royal Meteorological Society*, *147*(735), 1189–1201. https://doi.org/10.1002/qj.3966Dudhia, J. (1989). Numerical Study of Convection Observed during the Winter Monsoon Experiment Using a Mesoscale Two-Dimensional Model. *Journal of the Atmospheric Sciences*, *46*(20), 3077–3107. https://doi.org/10.1175/1520-0469(1989)046<3077:NSOCOD>2.0.CO;2Fischer, E. M., & Knutti, R. (2016).

Observed heavy precipitation increase confirms theory and early models. *Nature Climate Change*, *6*(11), 986–991. https://doi.org/10.1038/nclimate3110Fischer, E. M., Sippel, S., & Knutti, R. (2021). Increasing probability of record-shattering climate extremes. *Nature Climate Change*, *11*(8), 689–695. https://doi.org/10.1038/s41558-021-01092-9Fong, M., & Ng, L. K. (2012). *The weather and climate of Singapore*. Meteorological Service Singapore.Fowler, H. J., Lenderink, G., Prein, A. F., Westra, S., Allan, R. P., Ban, N., et al. (2021). Anthropogenic intensification of short-duration rainfall extremes. *Nature Reviews Earth & Environment*, *2*(2), 107–122. https://doi.org/10.1038/s43017-020-00128-6Guerreiro, S. B., Fowler, H. J., Barbero, R., Westra, S., Lenderink, G., Blenkinsop, S., et al. (2018). Detection of continental-scale intensification of hourly rainfall extremes. *Nature Climate Change*, *8*(9), 803–807. https://doi.org/10.1038/s41558-018-0245-3Gutmann, E. D., Rasmussen, R. M., Liu, C., Ikeda, K., Bruyere, C. L., Done, J. M., et al. (2018). Changes in Hurricanes from a 13-Yr Convection-Permitting Pseudo–Global Warming Simulation. *Journal of Climate*, *31*(9), 3643–3657. https://doi.org/10.1175/JCLI-D-17-0391.1Hibino, K., Takayabu, I., Wakazuki, Y., & Ogata, T. (2018). Physical Responses of Convective Heavy Rainfall to Future Warming Condition: Case Study of the Hiroshima Event. *Frontiers in Earth Science*, *6*, 35. https://doi.org/10.3389/feart.2018.00035Hong, S.-Y. (2006). Hongandlim-JKMS-2006. *Journal of the Korean Meteorological Society*, *42*, 129–151.Hong, S.-Y., Noh, Y., & Dudhia, J. (2006). A New Vertical Diffusion Package with an Explicit Treatment of Entrainment Processes. *Monthly Weather Review*, *134*(9), 2318–2341. https://doi.org/10.1175/MWR3199.1Kain, J. S. (2004). The Kain–Fritsch Convective Parameterization: An Update. *Journal of Applied Meteorology and Climatology*, *43*(1), 170–181. https://doi.org/10.1175/1520-0450(2004)043<0170:TKCPAU>2.0.CO;2Kusaka, H., Kondo, H., Kikegawa, Y., & Kimura, F. (2001). A Simple Single-Layer Urban Canopy Model For Atmospheric Models: Comparison With Multi-Layer And Slab Models. *Boundary-Layer Meteorology*, *101*(3), 329–358. https://doi.org/10.1023/A:1019207923078Kusaka, H., Suzuki-Parker, A., Aoyagi, T., Adachi, S. A., & Yamagata, Y. (2016). Assessment of RCM and urban scenarios uncertainties in the climate projections for August in the 2050s in Tokyo. *Climatic Change*, *137*(3), 427–438. https://doi.org/10.1007/s10584-016-1693-2Lauer, A., Zhang, C., Elison-Timm, O., Wang, Y., & Hamilton, K. (2013). Downscaling of Climate Change in the Hawaii Region Using CMIP5 Results: On the Choice of the Forcing Fields. *Journal of Climate*, *26*(24), 10006–10030. https://doi.org/10.1175/JCLI-D-13-00126.1Lenderink, G., & van Meijgaard, E. (2009). Unexpected rise in extreme precipitation caused by a shift in rain type? *Nature Geoscience*, *2*(6), 373–373. https://doi.org/10.1038/ngeo524Lenderink, G., & Meijgaard, E. van. (2010). Linking increases in hourly precipitation extremes to atmospheric temperature and moisture changes. *Environmental Research Letters*, *5*(2), 025208. https://doi.org/10.1088/1748-9326/5/2/025208Meehl, G. A., Goddard, L., Murphy, J., Stouffer, R. J., Boer, G., Danabasoglu, G., et al. (2009). Decadal Prediction: Can It Be Skillful? *Bulletin of the American Meteorological Society*, *90*(10), 1467–1486. https://doi.org/10.1175/2009BAMS2778.1Meyer,

L., Brinkman, S., van Kesteren, L., Leprince-Ringuet, N., & van Boxmeer, F. (2020). Technical Support Unit for the Synthesis Report, 169.Mlawer, E. J., Taubman, S. J., Brown, P. D., Iacono, M. J., & Clough, S. A. (1997). Radiative transfer for inhomogeneous atmospheres: RRTM, a validated correlated-k model for the longwave. *Journal of Geophysical Research: Atmospheres*, *102*(D14), 16663–16682. https://doi.org/10.1029/97JD00237Mukul Tewari, N., Tewari, M., Chen, F., Wang, W., Dudhia, J., LeMone, M., et al. (2004). Implementation and verification of the unified NOAH land surface model in the WRF model (Formerly Paper Number 17.5) (pp. 11–15). Presented at the 20th conference on weather analysis and forecasting/16th conference on numerical weather prediction.NCEP. (2021). NOAA Climate Data Record (CDR) of CPC Morphing Technique (CMORPH) High Resolution Global Precipitation Estimates, Version 1. Retrieved September 21, 2021, from https://www.ncei.noaa.gov/access/metadata/landing-page/bin/iso?id=gov.noaa.ncdc:C00948Pall, P., Patricola, C. M., Wehner, M. F., Stone, D. A., Paciorek, C. J., & Collins, W. D. (2017). Diagnosing conditional anthropogenic contributions to heavy Colorado rainfall in September 2013. *Weather and Climate Extremes*, *17*, 1–6. https://doi.org/10.1016/j.wace.2017.03.004Panthou, G., Mailhot, A., Laurence, E., & Talbot, G. (2014). Relationship between Surface Temperature and Extreme Rainfalls: A Multi-Time-Scale and Event-Based Analysis. *Journal of Hydrometeorology*, *15*(5), 1999–2011. https://doi.org/10.1175/JHM-D-14-0020.1Park, I.-H., & Min, S.-K. (2017). Role of Convective Precipitation in the Relationship between Subdaily Extreme Precipitation and Temperature. *Journal of Climate*, *30*(23), 9527–9537. https://doi.org/10.1175/JCLI-D-17-0075.1Prein, A. F., Liu, C., Ikeda, K., Trier, S. B., Rasmussen, R. M., Holland, G. J., & Clark, M. P. (2017). Increased rainfall volume from future convective storms in the US. *Nature Climate Change*, *7*(12), 880–884. https://doi.org/10.1038/s41558-017-0007-7Rajczak, J., & Schär, C. (2017). Projections of Future Precipitation Extremes Over Europe: A Multimodel Assessment of Climate Simulations. *Journal of Geophysical Research: Atmospheres*, *122*(20), 10,773-10,800. https://doi.org/10.1002/2017JD027176Rasmussen, R., Liu, C., Ikeda, K., Gochis, D., Yates, D., Chen, F., et al. (2011). High-Resolution Coupled Climate Runoff Simulations of Seasonal Snowfall over Colorado: A Process Study of Current and Warmer Climate. *Journal of Climate*, *24*(12), 3015–3048. https://doi.org/10.1175/2010JCLI3985.1Sato, T., Kimura, F., & Kitoh, A. (2007). Projection of global warming onto regional precipitation over Mongolia using a regional climate model. *Journal of Hydrology*, *333*(1), 144–154. https://doi.org/10.1016/j.jhydrol.2006.07.023Schär, C., Frei, C., Lüthi, D., & Davies, H. C. (1996). Surrogate climate-change scenarios for regional climate models. *Geophysical Research Letters*, *23*(6), 669–672. https://doi.org/10.1029/96GL00265Scherrer, S. C., Fischer, E. M., Posselt, R., Liniger, M. A., Croci-Maspoli, M., & Knutti, R. (2016). Emerging trends in heavy precipitation and hot temperature extremes in Switzerland. *Journal of Geophysical Research: Atmospheres*, *121*(6), 2626–2637. https://doi.org/10.1002/2015JD024634Shepherd, T. G. (2014).

Atmospheric circulation as a source of uncertainty in climate change projections. *Nature Geoscience*, *7*(10), 703–708. https://doi.org/10.1038/ngeo2253Simón-Moral, A., Dipankar, A., Doan, Q.-V., Sanchez, C., Roth, M., Becker, E., & Huang, X.-Y. (n.d.). Urban intensification of convective rainfall over the Singapore – Johor Bahru region. *Quarterly Journal of the Royal Meteorological Society*, *n/a*(n/a). https://doi.org/10.1002/qj.4147Taylor, K. E., Stouffer, R. J., & Meehl, G. A. (2012). An Overview of CMIP5 and the Experiment Design. *Bulletin of the American Meteorological Society*, *93*(4), 485–498. https://doi.org/10.1175/BAMS-D-11-00094.1United Nations. (2015). Sustainable Development Goals. Retrieved August 8, 2021, from https://www.undp.org/sustainable-development-goalsUnited Nations. (2018, May 16). 2018 Revision of World Urbanization Prospects Multimedia Library - United Nations Department of Economic and Social Affairs. Retrieved August 24, 2021, from https://www.un.org/development/desa/publications/2018-revision-of-world-urbanization-prospects.htmlvan Vuuren, D. P., Edmonds, J. A., Kainuma, M., Riahi, K., & Weyant, J. (2011). A special issue on the RCPs. *Climatic Change*, *109*(1–2), 1–4. https://doi.org/10.1007/s10584-011-0157-yWestra, S., Fowler, H. J., Evans, J. P., Alexander, L. V., Berg, P., Johnson, F., et al. (2014). Future changes to the intensity and frequency of short-duration extreme rainfall. *Reviews of Geophysics*, *52*(3), 522–555. https://doi.org/10.1002/2014RG000464World Bank. (2010). *Cities and Climate Change: An Urgent Agenda*. Retrieved from https://openknowledge.worldbank.org/bitstream/handle/10986/17381/637040WP0Citie00Box0361524B0PUB

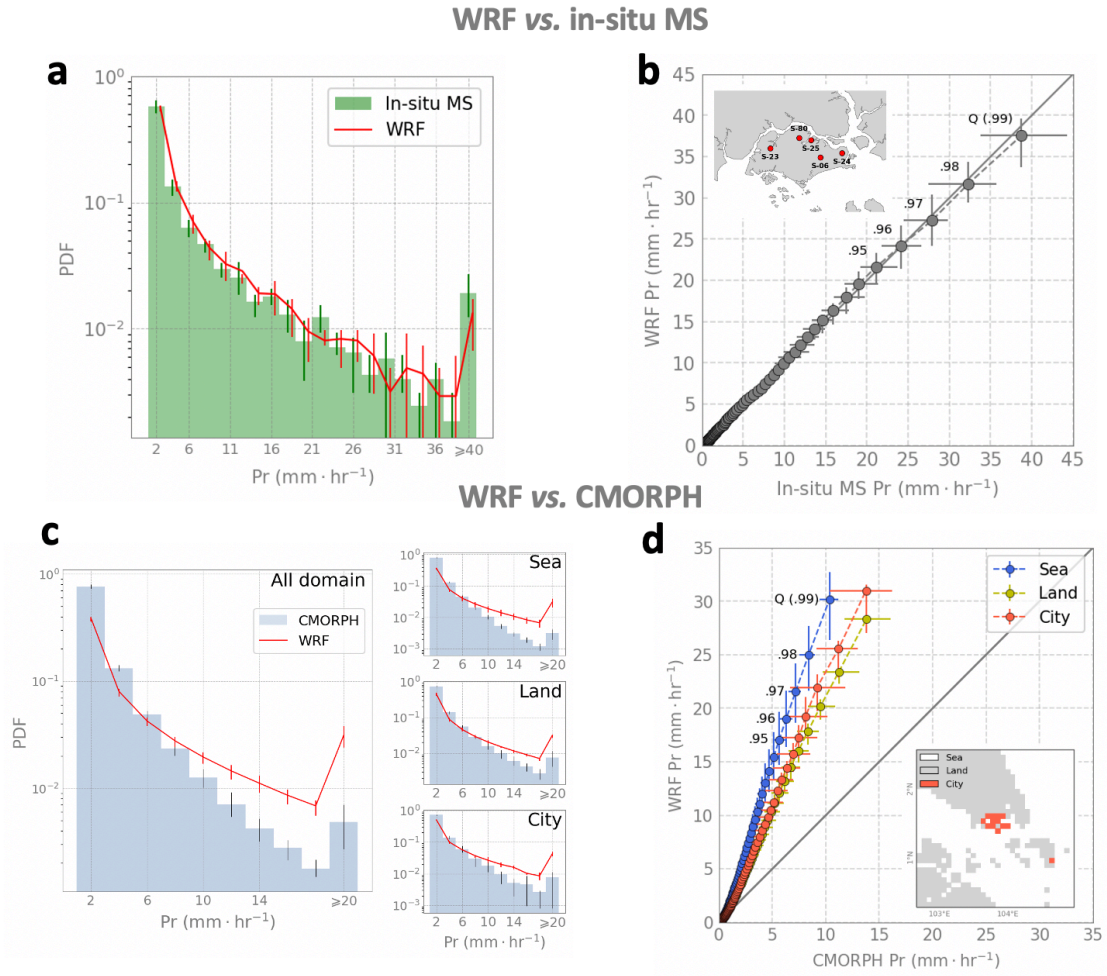

Figure 1. WRF performance against in-situ measurement and satellite-derived precipitation product. (a) Probability density function (PDF) of WRF simulations and in-situ measurements at six weather stations (see inset of b) run by the Meteorological Service Singapore. Results are averages across all stations of modelled (corresponding to the grid of the in-situ location) and observed hourly data in November for ten years 2005 – 2014. (b) Quantile-quantile (Q-Q) plot for WRF and in-situ measurement data. (c) PDF of WRF simulations and satellite-derived precipitation CMORPH analysis. Left panel is the average PDF of all grid cells in the domain of interest (inset map in d). WRF rainfall values are upscaled to match the spatial resolution of CMORPH data (approximately 8 x 8 km). Right panels show PDFs for different surface covers, i.e., sea, land, city, respectively. (d) Q-Q plot for WRF and CMORPH rainfall.

Uncertainty ranges shown in all panels indicate annual variability, i.e., the range between percentile 25 and 75 of annual values (10 years).

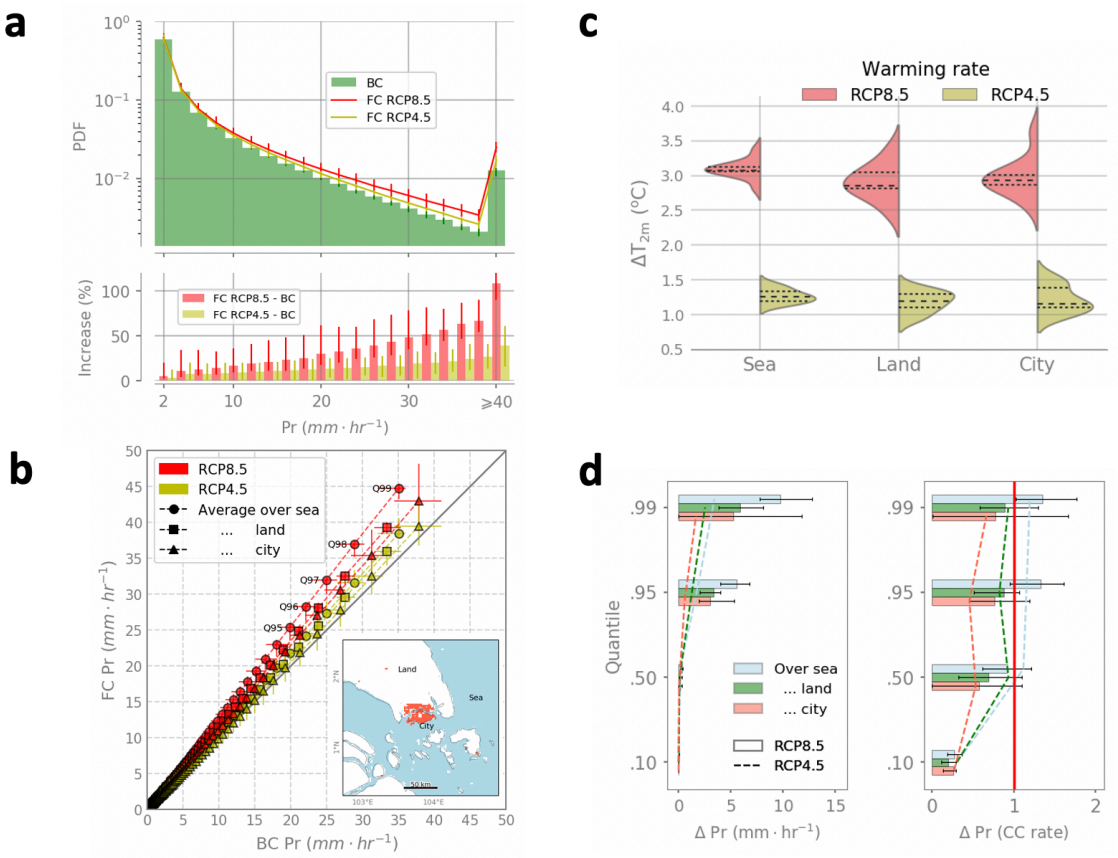

Figure 2. Extreme precipitation becomes more frequent and intense with global warming. (a) Probability density functions (PDFs) of baseline climate (BC) and future climate (FC) (upper sub-panel) and anomaly of FC relative to BC in percent (lower sub-panel). PDFs are whole-domain averages calculated from hourly precipitation (Pr) data for each grid cell. Quantile-quantile plot (b) for BC and FC for different land covers. Land area is defined as non-sea and non-urban areas in the domain of interest. Like PDFs, quantile values are the average of individual grid cell values. (c) PDFs of area-averaged temperature for three scenarios (BC and two FCs) for the entire domain, sea, land and city. (d) the FC-BC difference for sea, land, and city (upper subpanel); the FC-BC difference after Clausius-Clapeyron (CC) scaling (assuming a humidity increase of 7% per K warming.

Uncertainty ranges shown in all panels indicate annual variability, i.e., the range between percentile 25 and 75 of annual values (10 years).

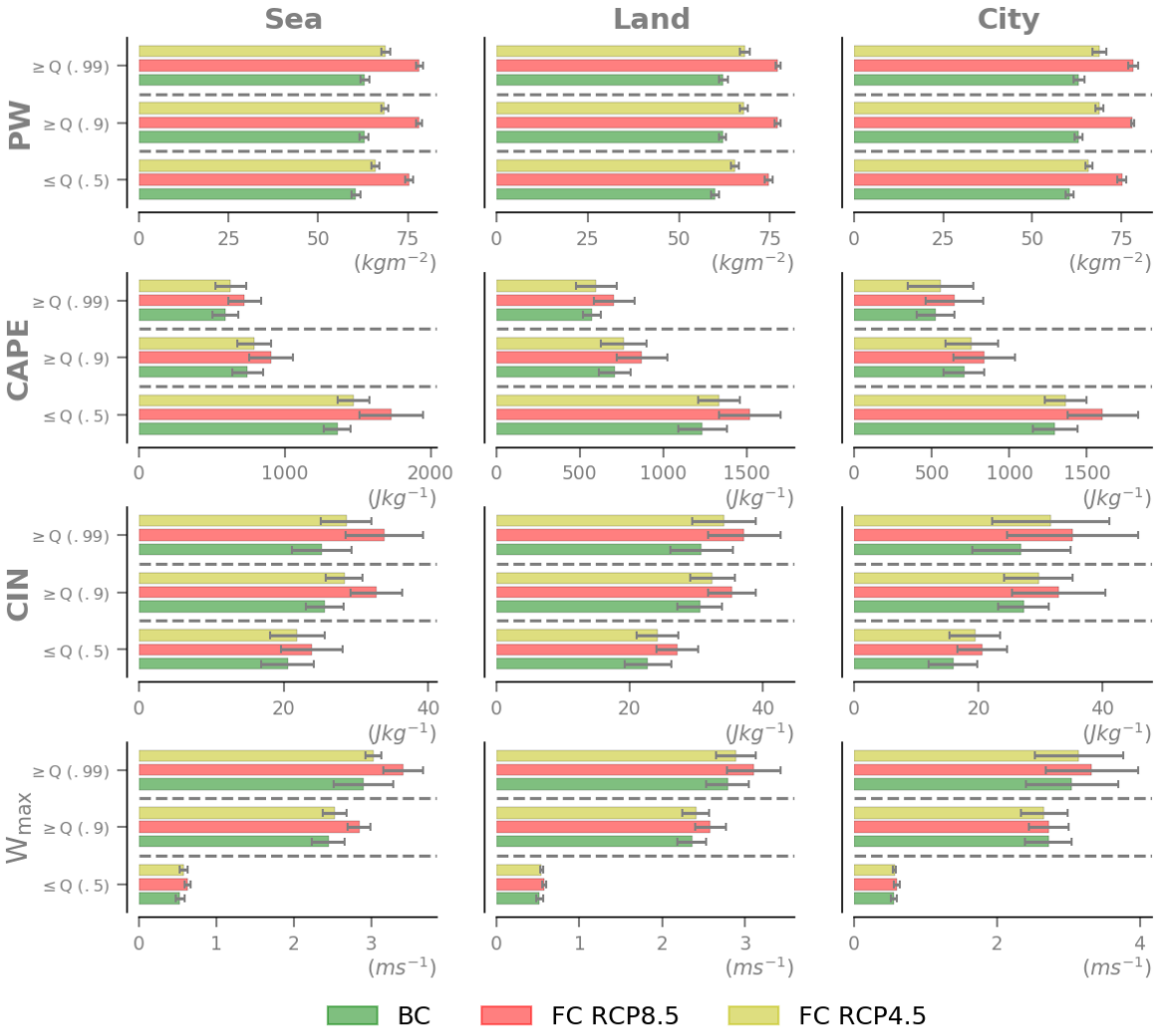

Figure 3. Change in atmospheric variables associated with precipitation. Shown are from top to bottom precipitable water (PW), convective available potential energy (CAPE), convective inhibition (CIN), and maximum vertical velocity (W_max) for three different land covers (left to right) and for three precipitation types, i.e., below quantile 0.5, above quantile 0.9, and 0.99. Values are area averages for the respective land covers. Different bar color indicates values of

BC, FC RCP8.5, and RCP4.5, respectively. BC is baseline climate (i.e., November 2005 – 2014), FC is future climate defined as 2080 – 2099. Uncertainty ranges shown in all panels indicate annual variability, i.e., the range between percentile 25 and 75 of annual values (10 years).

Table 1. Model configuration and physical scheme settings.

	Domain 01	Domain 02	Domain 03
Grid spacing	30.0 km	6.0 km	2.0 km
Number of grids	120 x 120	206 x 206	154 x 154
Number of vertical layers	35 layers		
Microphysics scheme	WRF single–moment 6–class scheme(Hong, 2006)		
Shortwave radiation	Dudhia Shortwave scheme(Dudhia, 1989)		
Longwave radiation	RRTM Longwave scheme(Mlawer et al., 1997)		
Boundary layer scheme	Yonsei university scheme(Hong et al., 2006)		
Land surface scheme	Noah land-surface model (Mukul Tewari et al., 2004)		
Urban canopy model	Single-layer urban canopy model (Kusaka et al., 2001)		
Cumulus	Kain–Fritsch scheme (Kain, 2004) (Domain 01 only)		

Table 2. List of initial and boundary conditions used for simulations.

Experiments	Description	Initial & boundary conditions
BC	Baseline Climate	ERA Interim, Novembers 2005 – 20
FC RCP8.5	Future climate up to 2080 – 2099 with scenario RCP8.5	CMIP5 RCP8.5 ensemble means (36
FC RCP4.5	Future climate up to 2080 – 2099 with scenario RCP8.5	CMIP5 RCP8.5 ensemble means (30

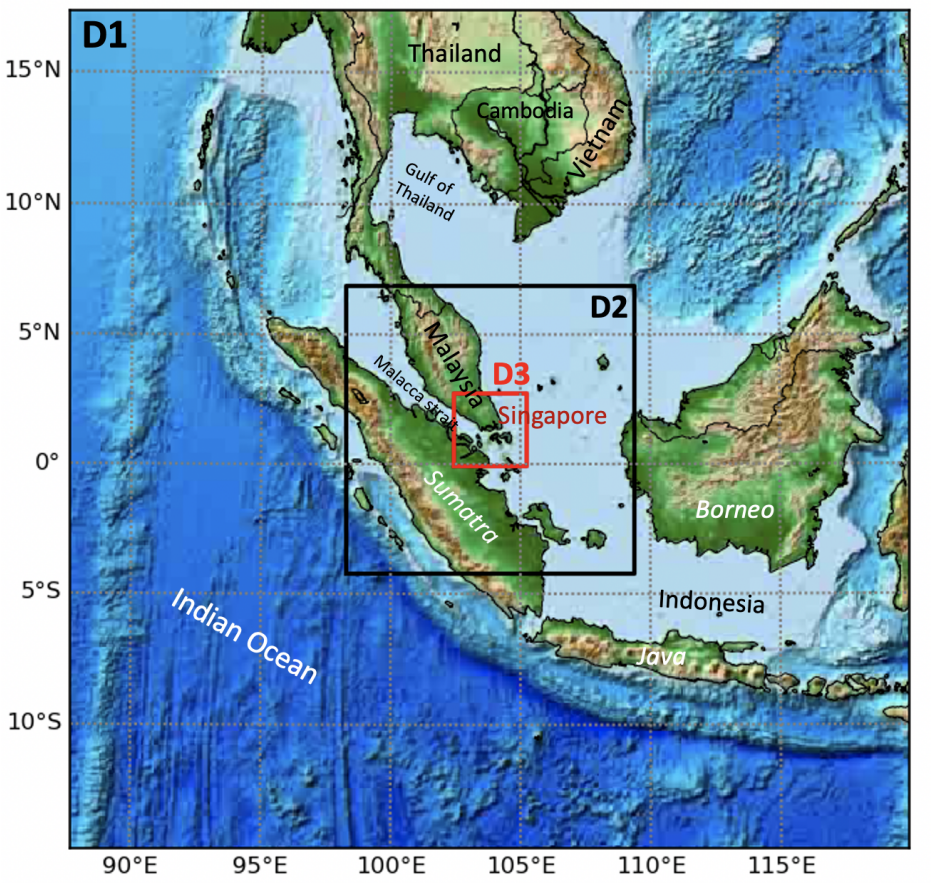

Figure S1. Domain configuration. Outermost, middle and innermost domains D1, D2, and D3 have a spatial resolution of 30 x 30, 6 x 6, and 2 x 2 km, respectively. D1 includes Singapore, Malaysia, parts of Indonesia, Thailand, and Vietnam. D2 covers the Malay Peninsula, parts of Sumatra. D3 is centered over Singapore and the southern part of the Malay Peninsula.

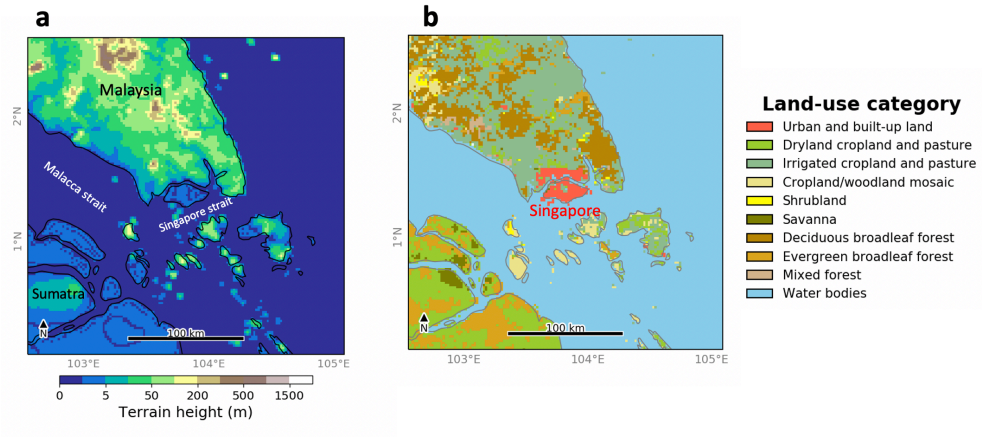

Figure S2. Surface conditions of inner most domain centered on Singapore. (a) map of topography height and (b) land cover with 2 x 2 km resolution.

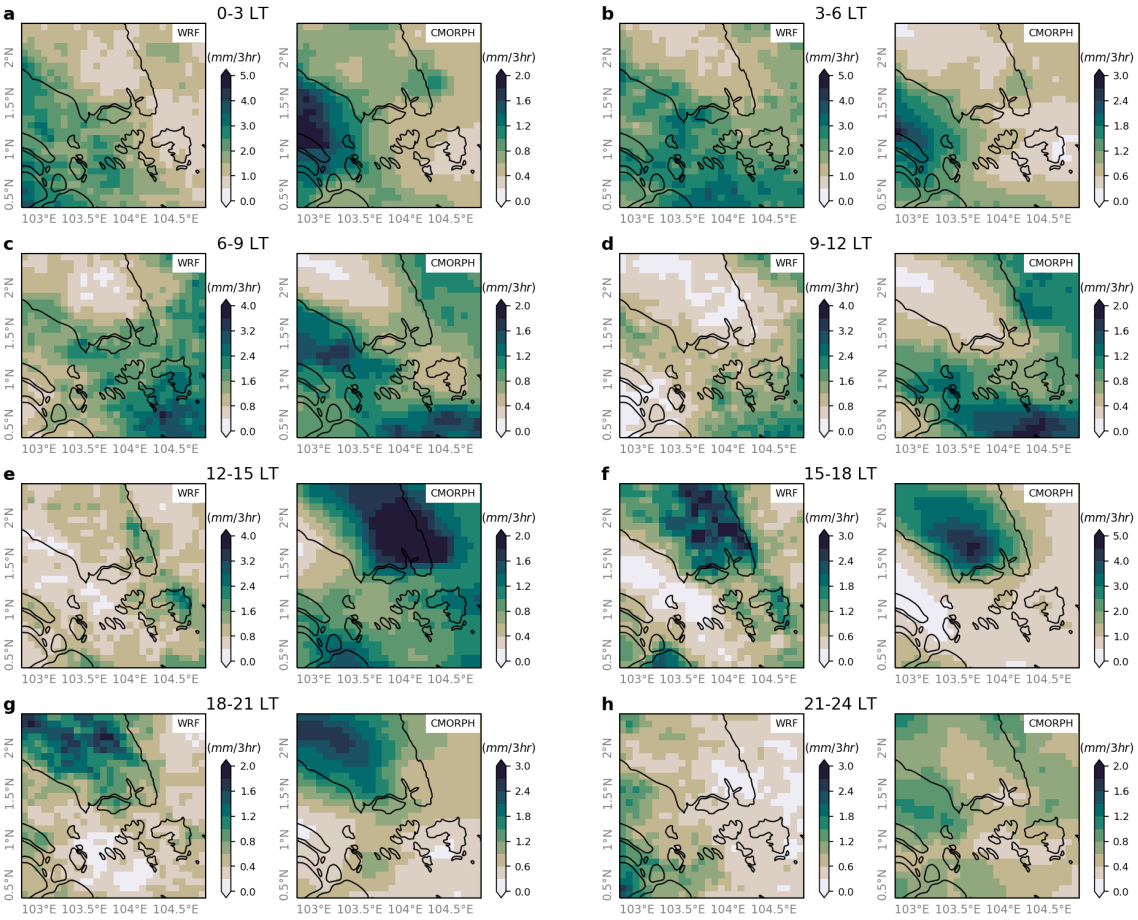

Figure S3. Distribution of rainfall over the Singapore region compared between WRF and CMORPH data. 3-hourly accumulated rainfall, averaged over November for ten years 2005 – 2014. Spatial resolution of data is unified to that of CMORPH data which is about 8 x 8 km.

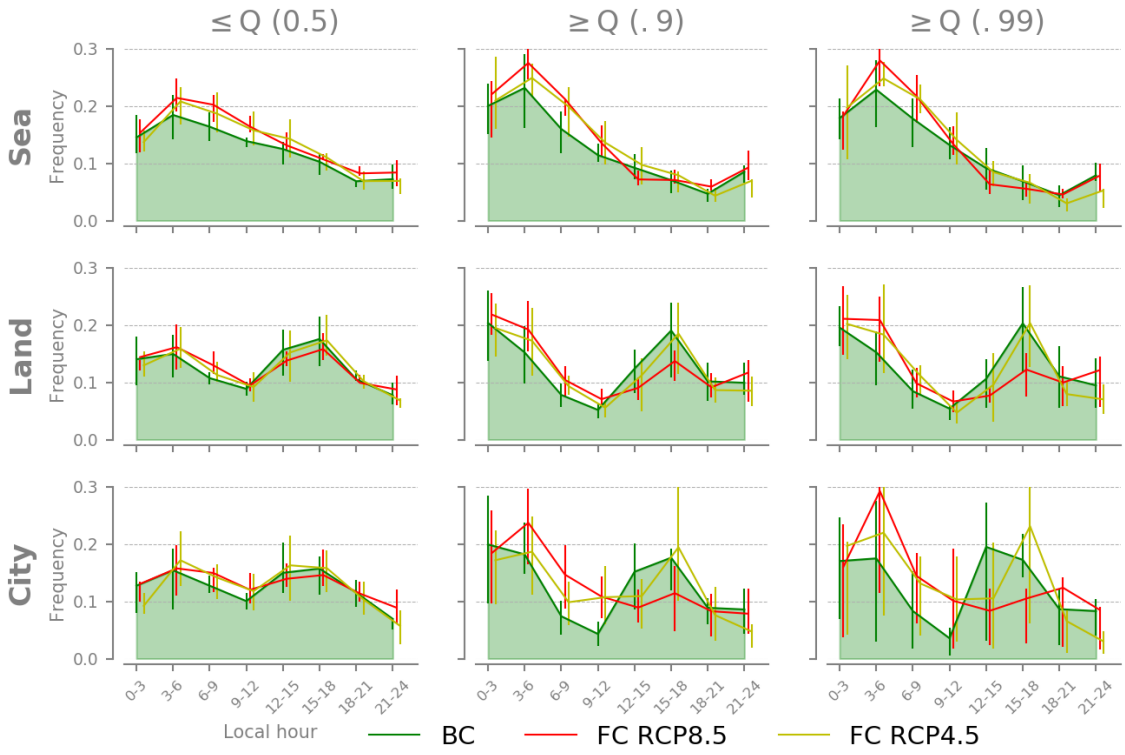

Figure S4. Timing of rainfall for different land covers, rain types and warming scenarios. A single peak is seen over water, but double peaks are present over land, with the early morning peak considered as a results of rainfall propagation from the ocean. Uncertainty ranges shown in all panels indicate annual variability, i.e., the range between percentile 25 and 75 of annual values (10 years).